

# Theta phase–specific codes for two-dimensional position, trajectory and heading in the hippocampus

John R Huxter, Timothy J Senior, Kevin Allen & Jozsef Csicsvari

Temporal coding is a means of representing information by the time, as opposed to the rate, at which neurons fire. Evidence of temporal coding in the hippocampus comes from place cells, whose spike times relative to theta oscillations reflect a rat's position while running along stereotyped trajectories. This arises from the backwards shift in cell firing relative to local theta oscillations (phase precession). Here we demonstrate phase precession during place-field crossings in an open-field foraging task. This produced spike sequences in each theta cycle that disambiguate the rat's trajectory through two-dimensional space and can be used to predict movement direction. Furthermore, position and movement direction were maximally predicted from firing in the early and late portions of the theta cycle, respectively. This represents the first direct evidence of a combined representation of position, trajectory and heading in the hippocampus, organized on a fine temporal scale by theta oscillations.

In the rat hippocampus, pyramidal cells fire in response to the animal's location in the environment<sup>1</sup>. By analyzing the momentary firing rates of many such place cells, it is possible to reconstruct the rat's current location<sup>2,3</sup>. In addition to this rate code, it has been proposed that neuronal activity can convey information depending on the timing of cell activity. One of the best demonstrations of such a temporal code is the theta phase precession of place cells. This is a monotonic (unidirectional) backwards shift in spike timing ('firing phase') relative to local 4–12-Hz theta-field oscillations<sup>4</sup> and is observed as a rat repeatedly crosses the cell's place field on a linear track<sup>5–8</sup>. Phase precession is a direct consequence of the fact that place cells tend to fire in rhythmic bursts in their place fields with an interburst frequency that is slightly higher than the frequency of local theta-field oscillations.

Phase precession imposes a temporal structure on the timing of those place cells representing overlapping places. On linear tracks, this makes firing phase a powerful means of representing absolute position<sup>9</sup>, relative position in the place field<sup>5,7</sup>, sequences<sup>6,10</sup> and possibly movement trajectories<sup>11</sup>. Firing phase is also dissociable from firing rate, enabling cells to potentially encode spatial and nonspatial aspects of experiences at the same time<sup>7,12</sup>. It is therefore unsurprising to us that phase precession has come to have a central role in many recent models of hippocampal plasticity, path integration and episodic memory<sup>6,11,13–15</sup>. Spike timing on theta timescales may also be involved in information processing beyond the hippocampus and may mediate the transfer of information between the hippocampus and neocortical structures<sup>16,17</sup>.

A better understanding of the mechanism and utility of phase precession critically depends on determining whether it is only present during stereotyped behavior or whether it is a more robust and generalizable phenomenon. However, there has only ever been indirect

evidence for monotonic phase precession on tasks in which the animal's trajectory is free to vary. Previously, examples have been shown of two cells for which firing began and ended on opposite halves of the theta cycle as the rat crossed place fields in a square box<sup>6</sup>. Others have focused on the temporal dynamics of firing phase during open-field exploration, and treated the relationship with position as a byproduct of the level of excitation of the neuron<sup>18</sup>. In both cases, however, the relationship between firing phase and position, or position relative to the cell's firing field, is ambiguous.

Indeed, whether true monotonic phase precession even occurs during open-field exploration, and what information it might encode, depends on the mechanism by which it is generated. For example, widely accepted 'look-ahead' models of phase precession<sup>11,13,19–21</sup> suggest that the phenomenon reflects the replay of cell firing sequences representing a previously experienced series of positions. But in open field exploration, the association of each position with many trajectories may cause cell firing to become independent of any one trajectory. Consequently, the cell might be expected to stop participating in phase precession<sup>22</sup>. Therefore, identifying the presence of monotonic phase precession during nonstereotyped behavior is an important step toward establishing its general utility for temporal coding and the mechanism by which it is generated. Furthermore, we set out to assess the different types of information represented by spike timing to better understand the means by which the hippocampus is involved in spatial-information processing.

## RESULTS

We trained six rats to randomly forage for food pellets in a circular arena. During foraging, we recorded the activity of 133 place cells and theta oscillations from the dorsal CA1 subfield of the hippocampus. To

MRC Anatomical Neuropharmacology Unit, Department of Pharmacology, University of Oxford, Mansfield Road, Oxford OX1 3TH, UK. Correspondence should be addressed to J.C. (Jozsef.csicsvari@pharm.ox.ac.uk).

Received 18 October 2007; accepted 7 March 2008; published online 20 April 2008; doi:10.1038/nn.2106

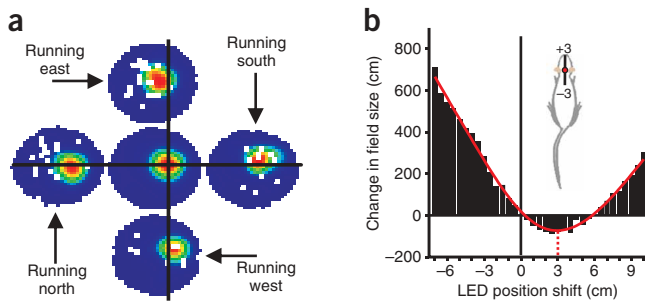


**Figure 1** Correcting discrepancy between LED position and perceived position. **(a)** A single place field defined using only spikes fired when the rat ran in one of four cardinal directions ( $\pm 30^\circ$ , as indicated by arrows) relative to the overhead camera. The average place map is shown in the middle. It is clear that firing shifts backwards along the rat's trajectory, suggesting either that the cell fires in anticipation of entering the place field or that the LED is placed too posterior on the rat's head. We assumed the latter. White pixels indicate places that the animal did not visit when running in the indicated direction. **(b)** The effect on mean place-field size of shifting the LED position along the axis of the rat's head. Data were averaged across all recorded place cells. Fitting a cubic spline to the data indicates a place-field minimum (red dotted line) is achieved with a 3-cm forward shift. Consequently for the current experiment, all position data were shifted forward by 3 cm before any further analyses were conducted. Given our LED position, a 3-cm shift suggests that the rat takes the position of its nose as its current location.

determine whether monotonic phase precession occurs on passes through place fields, we analyzed chunks of data aligned to the moment of place-field entry (runs). However, it was first necessary to correct for the fact that the light-emitting diode (LED) array indicating the rat's position may not match the rat's internal perception of its location. Offline, we shifted the tracked  $x$ - $y$  position along the axis of the rat's head to minimize place-field size, using the assumption that place cells are ideally tuned to a single point in two-dimensional space<sup>23</sup>. The smallest, least-smeared place fields were achieved with a 3-cm forward shift in the apparent LED array position, which would place the LED approximately over the rat's nose (Fig. 1). This was taken as the rat's 'true' position for all subsequent analyses.

### Firing phase as a function of distance and peak angle

A shift in firing from the ascending to the descending phase of the theta cycle could be seen on individual runs, regardless of trajectory or heading (Fig. 2a). Heading refers to the direction of motion of the rat, and not 'head direction' (see Methods). For session-averaged analyses, all spikes were assigned a theta firing phase, with zero corresponding to the positive-to-negative zero crossing of the theta oscillatory wave (Fig. 2b). The run distance for a given spike was the length of the trajectory between the most recent place-field entry position and the rat's current position when the spike occurred. Plotting theta firing phase against run distance revealed significant phase precession for traversals in each of four different compass directions (Fig. 2c). Hence, the theta timing of place cells represents a two-dimensional measure of distance traveled through the field. Most place fields are not perfect circles, so passes from different directions vary in length. To compensate for this and to better combine data from many place fields of different shapes and sizes, we analyzed firing phase as a function of directional rate zone (DRZ), a measure of firing-rate distance relative to the place field peak (Fig. 2d,e, see Methods). Briefly, DRZ reflects the session-averaged firing rate at a given position in the environment, being zero at the field peak and either  $-1$  or  $+1$  wherever the cell does

not fire. The sign of the DRZ is negative when the rat is heading toward the peak and positive when heading away. After combining data from all cells, we found that theta firing phase was negatively correlated with DRZ (mean linear-circular  $r = 0.066$ ,  $P < 0.05$  for 107 out of 133 cells; Fig. 2f,g). Therefore, firing phase depends not only on distance from the place-field center, but also on the direction of motion (heading) relative to it (peak angle; Fig. 2d). We found that the 3-cm position correction did not have a noticeable effect on phase precession with our LED configuration (Supplementary Fig. 1 online).

Next we asked whether theta phase precession in the open field was similar to the previously studied form of the phenomenon on the linear track. Data from 75 place fields (53 cells) recorded on the linear track showed the expected phase-precession profile (Fig. 3a). The population profile for our open-field data was similar in terms of its negative slope and the difference between the mean firing phase on place-field entry and exit, but was less linear (Fig. 3b). However, the similarity between the profiles was improved if, for the open field, we restricted analysis to fast, straight runs through the place-field center (Fig. 3b). These restricted runs more closely resembled behavior on the linear track, where convoluted passes through the field, or passes that exclude the place-field center, are virtually impossible. It is noteworthy that the total range of firing phases shown by a given cell spanned  $360^\circ$ ; the difference between the average firing phases on field entry and field exit was approximately  $180^\circ$ . This applies to both the linear track and the open field.

To quantify the difference between phase precession on the two types of task, we also defined linear-track phase precession using the DRZ measure (Fig. 3c). Open-field phase precession from restricted runs did not differ from linear-track phase precession (run distance,  $P \approx 0.605$ ; DRZ,  $P \approx 0.715$ ; ANOVA, Tukey's honest significant difference (HSD); Fig. 3d). However, all-runs open-field phase precession yielded lower  $r$  values than either of the linear-track measures ( $P < 0.001$  and  $P < 0.05$ , respectively, ANOVA, Tukey's HSD). The phase-precession profiles for the two linear track measures were almost identical and their mean  $r$  values were not significantly different ( $P > 0.999$ ) (additional analyses of the effect of different types of field passes on phase precession are presented in Supplementary Fig. 2 online).

In keeping with previous linear-track findings<sup>5,18</sup>, we also found that that firing phase could be predicted from run distance, the time elapsed since entering the field (run time) and the instantaneous firing rate of the cell (IFR). However, run distance and DRZ yielded significantly better correlations with theta firing phase than did the other measures (Supplementary Fig. 3 online). Moreover, we confirmed in the open field that, although momentary firing rates first rose and then fell as place fields were crossed, changes in firing phase were consistently negative (Supplementary Fig. 3). Hence, as on the linear track, phase precession is dissociable from momentary spike-train dynamics and so can encode information independently of the firing rate of the cell. This also confirms that in two-dimensional exploration, as on the linear track, monotonic phase precession is typical of individual place-field traversals.

### Temporal coding of trajectories

Next we tested whether phase precession during two-dimensional foraging allows place cells that fire together in a theta cycle to represent different trajectories according to their theta timing. This has been suggested previously on the basis of results from linear tracks, where there is no freedom for trajectory to vary<sup>10,11,24</sup>. We looked at the offset of the temporal cross-correlogram peak (CCGP) for different cell pairs<sup>11</sup>. Those with highly overlapping fields had the largest amplitude CCGPs centered on zero, indicating high cofiring probability at the same phase in each theta cycle (for example, Fig. 4a,b). For cell pairs

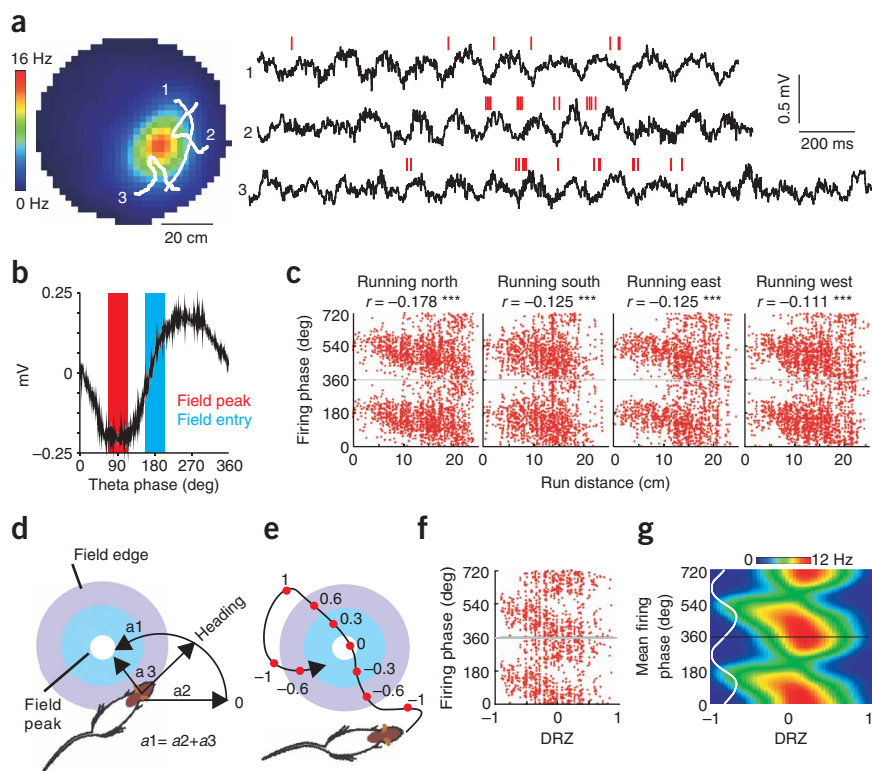


**Figure 2** Monotonic phase precession during random foraging. **(a)** A representative place field showing traces of three runs and corresponding CA1 theta-oscillatory field potential traces at right. Numbers mark the start of the runs. Red strokes indicate spike times of the cell, showing backward shifts in theta firing phase on each run. **(b)** Definition of theta phases illustrated against the mean detected theta cycle (one rat, one session) showing phase bands that were typical of field entry (blue,  $180^\circ$ ) and center (red,  $90^\circ$ ). **(c)** Firing phase versus distance traveled through the field in four directions ( $\pm 90^\circ$ ) for the cell in **a**. Distances are clipped at the 95th percentile. The y axis is doubled to aid visualization of the periodic phase distribution. \*\*\* indicates  $P < 0.001$ . **(d)** Peak angle ( $a_3$ ) is the degrees by which the rat would have to deviate from its current heading ( $a_2$ ) in order to run directly toward the field peak. **(e)** DRZ measures the distance from the place-field peak in terms of the mean firing rate at a given position (see Methods). DRZ was negative when the rat was approaching the peak (that is,  $a_3$  is between  $-90$  and  $+90$ ) and positive when moving away. **(f)** Combining data from all straight, fast runs through the place-field center (**Supplementary Methods**), DRZ phase precession spans  $\sim 360^\circ$ . **(g)** Population phase precession using the DRZ measure. Here the colors reflect the mean of the firing rate of cells from all rats as a function of both DRZ and theta firing phase.

that overlap less, the cofiring probability was reduced and the CCGP increasingly shifted away from zero. On runs from place field A to place field B, cell B tended to fire after cell A, and the reverse was true on runs from B to A (**Fig. 4c**). Therefore, the sequence of firing in a theta cycle represents a temporal code for the rat's trajectory, even under conditions where any trajectory is possible.

On the basis of this observation, we tested the relationship between field overlap and the magnitude of the CCGP shift for each cell pair

(**Fig. 4d**). For A-to-B runs, lower place-field overlap (greater field separation) was correlated with larger positive CCGP shifts (Pearson's  $r = -0.441$ ,  $P < 0.001$ ), whereas for runs in the opposite direction, lower overlap was correlated with more negative CCGP shifts (Pearson's  $r = 0.350$ ,  $P < 0.001$ ). Therefore, assuming we could record from all place cells firing in a given theta cycle, their temporal order would reflect all of the intermediary positions along the rat's current trajectory.

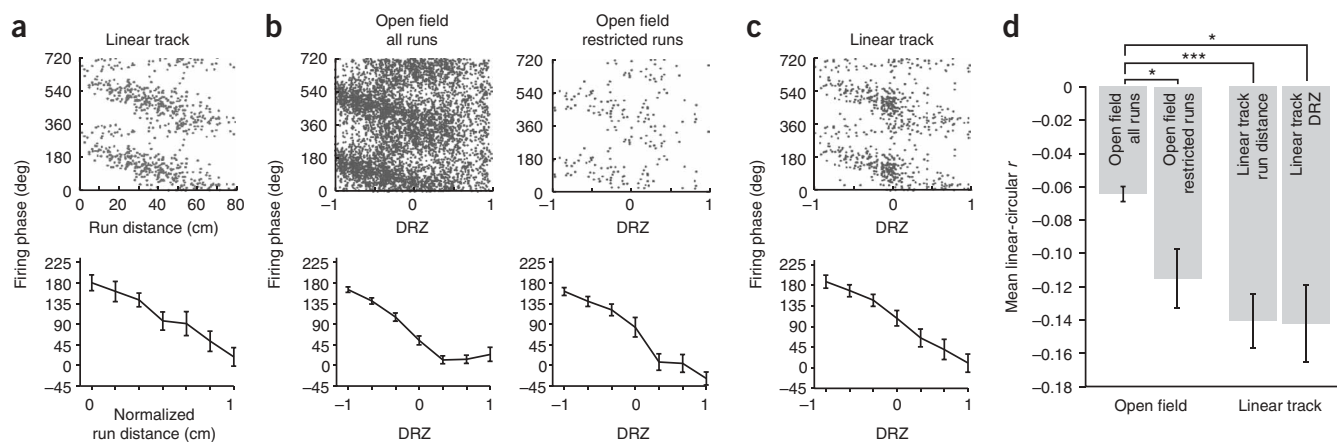


**Figure 3** Comparison with phase precession on the linear track. **(a)** Phase precession on the linear track from a typical place cell (top) and from the population average (bottom). Phase is plotted as a function of the distance traveled through the place field. The scatter plot is doubled along the y axis to aid visualization of the circular angle data. Population data are normalized to the size of each place field after removal of outliers above the 95th percentile and sorted into seven bins to create a phase-precession profile. **(b)** Phase as a function of DRZ in the open field, as shown by a different place cell (top) and the corresponding population profile (bottom). Plots on the left include data from all place-field crossings from all directions. Plots on the right use data restricted to straight, fast runs through the middle of the place field (see Methods). **(c)** Linear-track phase precession using the DRZ measure with the same cell as in **a** (top) and the corresponding population profile (bottom). The density of spikes near the field peak is partly because of the nonlinear nature of firing-rate changes as a place field is crossed. **(d)** Mean linear-circular correlation values for phase precession in the open field (left) and on the linear track (right). Only open-field phase precession based on the inclusion of all runs differed from the other measures. Error bars represent s.e.m. \* $P < 0.05$ , \*\*\* $P < 0.001$ , Tukey's HSD.

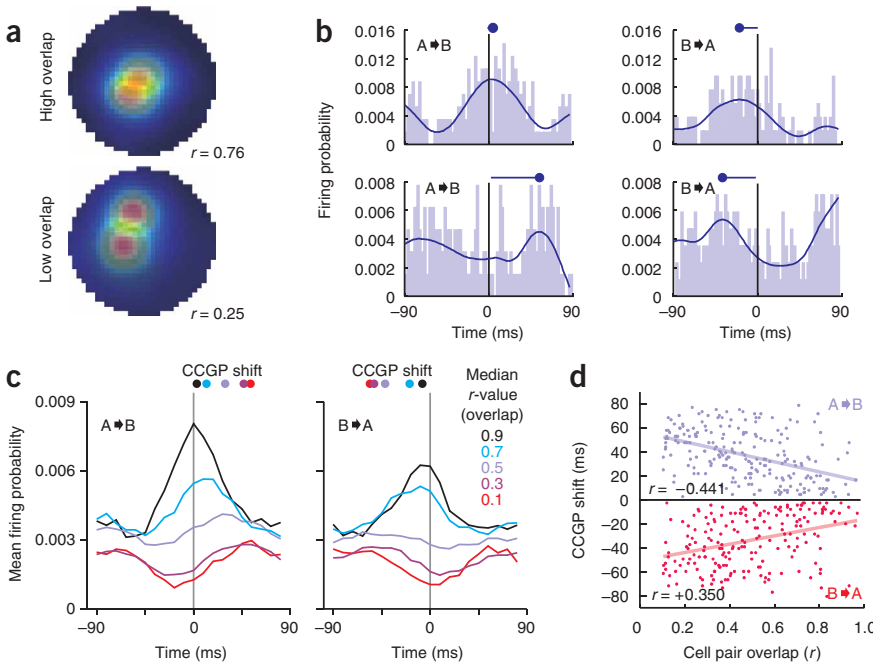


**Figure 4** Shifts in the CCGP for cell pairs indicate trajectory. **(a)** An example of cell pairs with high (top) and low (bottom) degrees of place field overlap.  $r$  is the similarity between the two fields (spatial correlation, see Methods). **(b)** Cross-correlograms of spike times for cell B relative to cell A for the high (top) and low (bottom) overlap pairs from **a**, and for runs from A to B (that is, when the rat entered place field A first) and B to A. Curves are cubic spline fits used to establish the nearest-to-zero CCGP (filled circles). The CCGP shift is positive on runs from A to B and negative on runs from B to A. **(c)** Average cross-correlograms for cell pairs categorized by overlap (median  $r$  value for cell pairs in each category). CCGP shift (filled circles aligned to peaks) increased as field overlap decreased. **(d)** The field overlap and CCGP shift for runs from A to B (purple) and B to A (red) are shown for different cell pairs together with the linear regression line. Note the significant correlations for both cases. Solid lines represent least-squares fit for each set,  $P < 0.001$  for both.

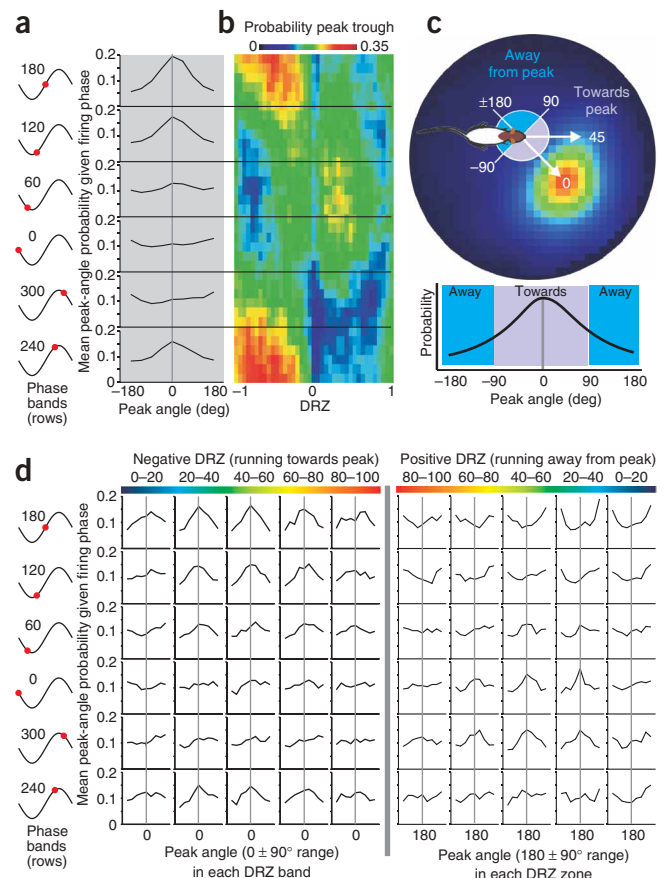
**Probability-based reconstruction of movement direction**

With our results demonstrating that the theta firing-phase relationships between cells encode trajectory, it follows that there is a directional component to the timing of place-cell firing. Thus, we reasoned that the combined rate and theta phase of cells may encode the rat's heading direction. To test this, we calculated for each spike the change in heading required for the rat to run straight toward the cell's place-field center (peak angle; **Fig. 2d**). We calculated the probability of firing at different peak angles, given that firing occurred in one of six different theta-phase bands. We found that when a cell fires on the ascending slope (theta phase  $180 \pm 30^\circ$ ), the rat tends to be heading directly toward the field center (peak angle =  $0^\circ$ ), whereas firing on the descending slope (theta phase  $300^\circ \pm 30^\circ$ ) weakly predicts motion  $180^\circ$  away from the peak (**Fig. 5a**). However, inference of peak angle from the probability of firing at a given theta phase also varies depending on the proximity to the place-field peak, as measured by DRZ (**Fig. 5b–d**). Peak angle is more prone to noise the closer the rat is to a given place-field center, and cannot be defined at all directly at the center. Indeed, the tuning curves flatten near the middle of the place

field, indicating that the ability to predict heading relative to the place field is weaker when the rat is near the peak (**Fig. 5b–d**).

The peak-angle tuning curves provide evidence of field-centered directional information in the hippocampus, which may in turn provide information about the rat's movement direction (heading) in real-world coordinates. To test this hypothesis, we used the tuning

**Figure 5** Theta firing phase reflects peak angle. **(a)** For all cells, given firing at a particular theta phase (six bands, left), the probability that a rat is running at a particular angle relative to the place-field peak (peak angle, right) is shown. The rat is most likely to be running toward the field center when cells fire at phase  $180^\circ$ . Conversely, firing at phase  $0^\circ$  weakly predicts movement away from the peak. **(b)** Peak-angle prediction strength as a function of firing phase (36 bands) and DRZ. Low prediction power (blue) arises from flat peak-angle probability histograms. Note the high prediction power (red and yellow) in firing phase bands near the ascending portion of the theta cycle. Peak angle is ambiguous at the peak itself (vertical midline). **(c)** Data in **d** were treated separately for motion toward (negative DRZs, purple) and away from (positive DRZs, blue) the place-field peak. For positive DRZs, the blue portions of the histograms (see example, bottom) were swapped and pushed together to form a single continuous histogram with a midpoint indicating motion directly away from the place-field peak ( $\pm 180^\circ$ ). **(d)** Mean firing-probability histograms for each of ten firing-rate zones (columns) and each of six  $60^\circ$ -wide firing-phase categories (rows, defined at left). Histograms for negative DRZs are centered at  $0^\circ$ , whereas those for positive DRZs are centered at  $180^\circ$ .



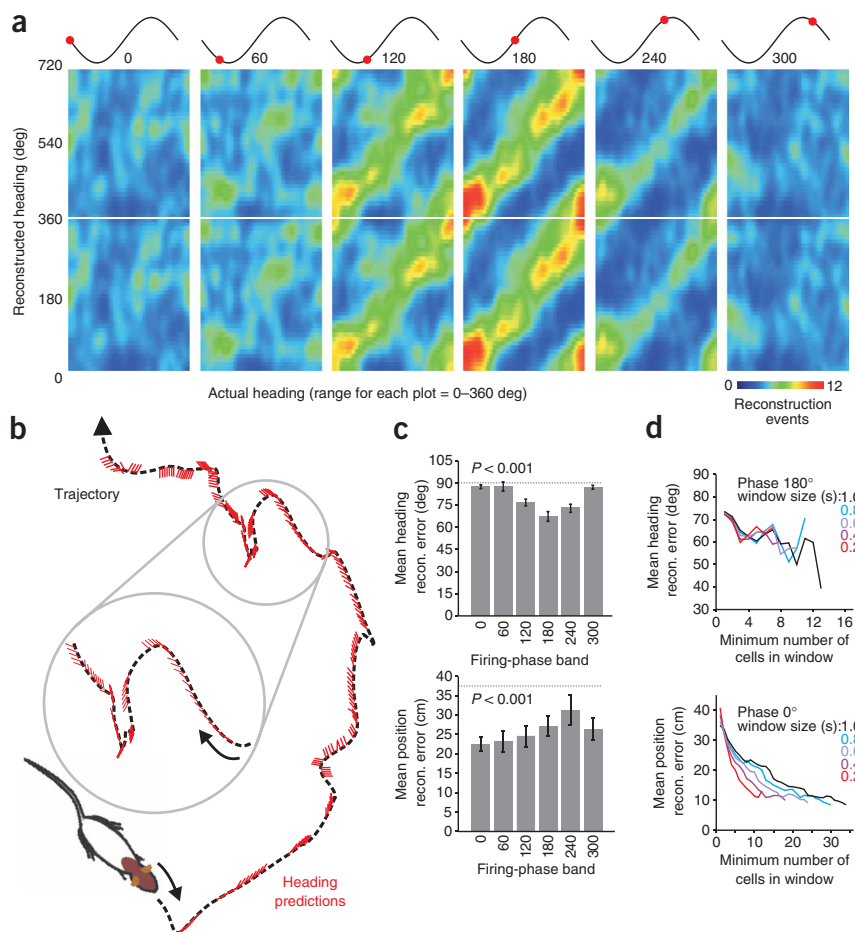


**Figure 6** Using firing phase to predict heading. **(a)** Density plots for actual versus predicted heading in world-centered coordinates averaged across rats on the basis of spikes fired in each of six theta-phase bands. Each plot is a  $72 \times 72$  matrix of prediction event counts, smoothed with a  $7 \times 7$  Gaussian kernel. Plots are doubled along the y axis. Sinusoids indicate the median firing phase of spikes in each band on a hypothetical theta wave. **(b)** Sample movement path of the animal (trajectory, black line) for a 10-s period, with heading predictions indicated by red strokes (based only on spikes firing in the  $180^\circ$  phase band, minimum two spikes per prediction). Inset, an enlarged portion of the trajectory showing good prediction when the animal turned sharply. **(c)** Mean reconstruction errors for heading (top) and position (bottom) based on spikes fired in each phase band. Heading and position reconstruction are optimized in bands at opposite phases of theta cycles. Values are averages across rats. Error bars represent s.e.m. Dotted line represents chance.  $P < 0.001$  (ANOVA). **(d)** Prediction errors are reduced as a function of the number of cells in the prediction window. Top, heading prediction, phase band  $180^\circ$ . Bottom, position prediction, phase band  $0^\circ$ . Using larger window sizes (line colors) increased the potential number of cells in the window and hence the potential for good prediction, but introduced larger baseline error related to the movement of the rat in the window. A 400-ms window was used for all other analyses.

curves to construct a Bayesian heading-prediction model (see Methods and **Supplementary Fig. 4** online). Cross-validation was applied, using the first half of each session as the training set and the second half for testing prediction. Prediction quality depended on spike-phase band (repeated-measures ANOVA,  $F_{5,25} = 17.427$ ,  $P < 0.001$ ). Firing anywhere on the ascending slope of theta (phase categories  $120^\circ$ ,  $180^\circ$  and  $240^\circ$ ) provided good heading prediction (**Fig. 6a**), even on very complicated trajectories (**Fig. 6b**). For these phase bands, mean reconstruction errors fell below chance levels (mean prediction error plus 95% confidence interval  $< 90^\circ$ ; **Fig. 6c**).

### Bayesian reconstruction of position

If heading is best predicted on the ascending slope of theta, we hypothesized that current position may be best predicted from the remaining portion of the cycle. To test this, we compared the accuracy of position reconstruction based on spikes fired at different theta phase bands using a Bayesian maximum-likelihood method<sup>3,9</sup>. Cross-validation was used in this case as well, and, as with heading prediction, position reconstruction varied across firing-phase bands (repeated-measures ANOVA,  $F_{5,25} = 7.418$ ,  $P < 0.001$ ), with the lowest errors (22 cm) being in the  $0^\circ$  band (**Fig. 6c**). For the  $240^\circ$  band, position reconstruction was not significantly better than chance (mean error plus 95% confidence interval  $> 35.5$  cm =  $1/2$  the cylinder diameter). Therefore, heading and position are best predicted from spikes at opposite phases of theta. As described previously<sup>6,18,25</sup>, this is consistent with observations that spikes occurring on the ascending slope and the trough of theta are broadly distributed around the edge and center of place fields, respectively (**Supplementary Fig. 5** online).

that we do not apply additional correction to prevent ‘jumpy’ predictions. However, for the reconstruction of both heading and position, reconstruction error in the optimal phase bands ( $180^\circ$  and  $0^\circ$  respectively) was inversely related to the number of cells in each 400-ms window (**Fig. 6d**). Therefore, recording from a sufficient number of cells would probably reduce reconstruction errors to the levels of measurement error.

### DISCUSSION

We have demonstrated that phase precession is not restricted to linear-track procedures, but occurs during unconstrained two-dimensional foraging as well. We also provide, to the best of our knowledge, the first confirmation that spike timing in theta cycles serves as a temporal code for the rat’s current trajectory and that both position and heading can be predicted from cell firing at different phases of the theta cycle. Phase precession on linear tracks imposes theta-timescale ordering onto neuronal spike trains and can therefore serve as a powerful means of inducing the synaptic plasticity required for the formation of spatial or episodic memory<sup>6,19,20</sup>. However, the general validity of this argument depends critically on the phenomenon’s independence from linear-track training regimes where behavior is very stereotyped. This has not been convincingly demonstrated until now.

### Monotonic phase precession during open-field exploration

We found that the relationship between the firing phase and DRZ was significant for 80% of our place cells, making two-dimensional phase precession typical of the place-cell population. There are strong similarities between linear-track and open-field phase precession.

First, the phase shift is negative in all parts of the place field in both procedures, indicating a dissociation of firing phase from the firing-rate output of the cell. Second, firing phases span approximately  $360^\circ$  of theta, but the average difference between firing phase at the beginning and end of phase precession is about  $180^\circ$ . This is consistent with the  $180^\circ$  shift in firing phase that is predicted from the interference of two detuned oscillators<sup>5</sup> and leaves open the possibility that other factors such as cell assembly dynamics may influence the exact phase at which cell spiking begins and ends<sup>11,26</sup>. Third, although phase precession occurs in all DRZs, variance in firing phase is much higher as the rat exits and the rate of change approaches zero at the departing edge of the field. This suggests that there is a possible role for spike-train dynamics or network interactions in constraining firing phase as the rat is approaching the field center<sup>27</sup>, or that firing phase changes are governed by different processes in the early and late parts of the theta cycle<sup>28</sup>.

### Phase precession provides a temporal code for trajectory

Previous work has shown that the relative timing of cell firing in theta cycles produces compressed representations of the series of positions the rat passes during stereotyped running<sup>6,10,11</sup>. On these narrow-track tasks, however, most positions can only be a part of two trajectories, and most place cells are only active on one of them<sup>29</sup>. We have demonstrated that when the rat's trajectory is free to vary, the relative timing of place-cell pairs in theta cycles can be used to distinguish the current trajectory from alternatives. Consequently phase precession represents a temporal code for the sequence of positions (that is, trajectory) and not simple reactivation of a single frequently repeated sequence. Temporal sequences at compressed time intervals are thought to facilitate plastic processes<sup>30,31</sup> by producing spiking intervals that fall below the deactivation time constant of NMDA receptors<sup>19,32,33</sup>. Phase precession can therefore be thought of as a hippocampal 'rehearsal' for sequences and a means of enhancing memory for particular trajectories or episodic-like events<sup>34</sup>.

### A heading signal in the hippocampus

We found that heading information can be encoded by place-cell firing on the ascending slope of theta oscillations. Conversely, the best position prediction was obtained from spikes fired at the descending slope and trough, as predicted from previous modeling work<sup>20</sup>. Attractor network models of path information<sup>13,35,36</sup> require a signal to move the peak of activity from the cell assembly representing the current location (cells firing together at the theta trough<sup>11</sup>) to that representing the next location along the current trajectory. Previously, movement of the attractor peak has been attributed to a combination of head-direction input and a signal representing speed of motion. Our results show that, in addition to a head-direction signal arising from the dorsal presubiculum<sup>37</sup>, the hippocampus could provide a re-entrant heading correction to a path integrator system based in the entorhinal cortex<sup>12,38</sup>. Indeed, lesions of the hippocampus have been linked to deficits in angular path integration<sup>39,40</sup>. The major targets of the CA1 region, the subiculum and the deep layers of the entorhinal cortex, also have directional firing properties<sup>38,41</sup> that may be derived from the hippocampal field-centered directional output. We note, however, that the presubiculum provides a more explicit head-directional signal to the entorhinal cortex, so the relative contribution of the hippocampus to directional firing in the entorhinal cortex is unknown.

A broad theta-timescale division in the encoding of qualitatively different information could allow selective sensitivity to position or heading information in structures downstream of the hippocampus, provided that the target 'listened' at the correct phase of theta. Certainly

the theta timing of inputs to the hippocampus has a large effect on their probability of spike transmission and the ability of the inputs to induce synaptic plasticity<sup>42,43</sup>. Recent evidence of theta-phase coordination between the hippocampus and the prefrontal cortex<sup>16,17</sup> supports the hypothesis that theta timing of hippocampal output is important for downstream processing. Others have reported that increased GABA<sub>B</sub> receptor-mediated inhibition early in each theta cycle (near the trough) selectively blocks input from CA3, but not entorhinal cortex<sup>20</sup>. The implication is that trough firing in CA1 reflects primarily current position information from the entorhinal cortex, whereas firing on the ascending slope also includes a predictive future location component derived from the CA3 recurrent network. This is consistent with our observation of better than chance position prediction across the entire theta cycle, but accurate heading prediction only on the ascending slope.

### Application to models of phase precession

Look-ahead models of phase precession assume that spatial inputs early in each theta cycle initiate firing in a chain of cells representing a previously learned sequence<sup>11,13,19,20</sup>. Assuming cell assemblies are bound according to the rules governing spike timing-dependent plasticity (STDP), the learned sequence establishes the asymmetric synaptic weights required to ensure replay in the correct direction on subsequent visits. In open-field exploration, however, a given position is associated with many trajectories, so cell assemblies representing the environment cannot be formed via STDP. Moreover, phase precession ought not to occur at all, as all possible trajectories have equal probability of being reactivated<sup>22</sup>. In contrast to this prediction, we observed both phase precession and temporal representation of trajectories in the open field, suggesting that synaptic weights in the network reflected place-field proximity<sup>44</sup>, not trajectories. This can be reconciled with look-ahead models of phase precession, provided a directional input temporarily alters the weights to reflect the current trajectory<sup>13,45</sup>.

Alternatively, detuned oscillator models can explain the emergence of phase precession without requiring learning to establish weights in the cell assembly network and are therefore consistent with open-field phase precession. These models suggest that phase precession occurs because spatial inputs to place cells cause them to begin firing rhythmic bursts at shorter intervals than the period of local theta-field potentials<sup>5,46</sup>. The interference pattern between the theta-field oscillation and a second oscillatory determinant of firing creates the phase-precession profile and, hence, the within-cycle timing of place cells. The second oscillator may arise from intrinsic membrane-potential dynamics of individual cells, or, as recently suggested, from the interaction of oscillating assemblies of place cells<sup>8</sup>. It was also demonstrated that the interburst interval of place cells is tightly correlated with running speed, consistent with the speed invariance in the relationship between firing phase and position in the place field<sup>5,7</sup>. However, detuned oscillator models cannot easily account for all observations, such as the preservation of phase-position correspondence on the linear track following disruption of theta oscillations in CA1 or the overlapping ('stacked') phase-precession profile observed for some place cells with dual firing fields<sup>21</sup>.

These issues could be resolved if hippocampal phase precession is inherited from detuned oscillator dynamics in upstream structures such as the entorhinal cortex<sup>25,45,47</sup>. Given that theta-field oscillations arise from periodic inhibition of pyramidal cells by GABAergic interneurons<sup>48</sup>, it is also likely that an interaction between running speed-dependent inhibition and excitation is involved in modulating the firing phase of place cells<sup>8,18,27,49</sup>. Indeed, changing excitability of place cells in theta cycles could explain the change in phase variance that we

observed from the early to the late portion of phase precession. And finally, we do not exclude the possibility that look-ahead models partially explain phase precession on linear tracks. That is, on stereotyped running tasks, a dual oscillator mechanism may be responsible for initially establishing phase precession, but, with experience, the plasticity that it facilitates could lead to an increasingly important role for look-ahead network dynamics.

## METHODS

**Surgery.** All procedures were carried out under an approved project license and in accordance with the Animals (Scientific Procedures) Act, 1986 (UK). We implanted six male Long-Evans rats with 16 independently moveable tetrodes that were positioned above the right dorsal hippocampus. After 7 d of postoperative recovery, rats were reduced to and maintained at 85% of their age-matched preoperative weight. Water was available *ad libitum*. During this period, we lowered the electrodes to the CA1 region of the dorsal hippocampus.

**Training and data acquisition.** Wide-band (0.1 or 1 Hz to 5 kHz) recordings of local field potentials and multiple-unit activity were amplified 1,000-fold using a 64-channel amplifier (Sensormium) and continuously digitized at 20 kHz using a 64-channel analog-to-digital converter computer card (United Electronics Industries). An array of three LED clusters was used to track the location and head direction of the animal (25 frames per s) via an overhead video camera (Sony). Recordings were made while the rat foraged for randomly dropped food pellets in a gray, cylindrical arena that was 75 cm in diameter, 51 cm high and enclosed by a 2 m in diameter black curtain to control distal visual cues. The rats were trained on the pellet-chasing task at least 30 min per d for at least 4 d before we collected data for analysis. If a rat stopped searching for pellets for more than 2 min, it was removed from the cylinder to reduce the association of the environment with nonforaging behavior. During training, the rats were screened for cells (**Supplementary Methods** online) and learned to spend virtually the entire time in the cylinder searching for food.

**Two-dimensional phase precession.** Phase precession was assessed by the linear-circular correlation between firing phase and each of four predictors: run distance, run time, IFR and DRZ. A run through a place field began the moment the field was entered and ends when the field is exited again. If tracking was lost in the field, the run was not included. IFR is the boxcar-averaged interspike interval in a 250-ms time window centered on a given spike. Run time is the time elapsed since the rat last entered the place field. Run distance is the summed distance between the position samples collected since the place field was entered. DRZ is a measure of distance from the peak, corrected by the rat's heading relative to the place-field peak. Note that by heading, we do not mean the direction in which the rat's head is pointing, but the rat's direction of motion. Although the two are almost identical on linear-track tasks, they frequently differ when the rat is sweeping its head left and right in search of food pellets. DRZ is defined as  $d(1 - \frac{r}{p})$ , where  $r$  is the mean firing rate in the rate-map bin corresponding with the rat's current position,  $p$  is the firing rate in the highest-rate bin of the map, and  $d$  is  $-1$  when the angle separating the rat's heading from the peak bin is less than  $90^\circ$  or  $+1$  if the angle is greater than  $90^\circ$ . The rate zone will be  $-1$  or  $+1$  when the rat is in regions where the cell does not fire and zero at the peak bin. Therefore, on a pass through the middle of the place field, the distance from the peak will decrease and then increase and the 'map' firing rate will increase and then decrease, but the DRZ will shift linearly from  $-1$  to  $+1$ . DRZ is, in this respect, analogous to distance traveled through the field, irrespective of direction and scaled to the size of the field. After removing predictor outliers (upper 5%), we calculated linear-circular correlations with firing phase<sup>50</sup> and looked at the proportion of cells for which the correlation was significant ( $P < 0.05$ ).

To determine whether spike-train dynamics influence changes in firing phase, we compared the temporal derivative (rate of change) of IFR and firing phase in each DRZ. The temporal derivatives were calculated by smoothing values with a sliding 3-theta-cycle window and then taking the difference in smoothed values between consecutive cycles.

**Linear-track phase precession.** One extra rat and three of the rats trained in the open field were also trained to shuttle for food delivered at either end of an

elevated linear track that was 180 cm long and 10 cm wide. These sessions were conducted in the same room as the open-field sessions and data were collected in the same way, but from a completely different set of cells. The track was oriented horizontally (east to west) as viewed from the overhead camera and treated as a one-dimensional environment by collapsing position data to a single pixel in the north-south dimension. We compared the coherence for place fields from the same cells before and after collapsing the data. The coherence (coh) measures were strongly correlated, but were higher for the collapsed data ( $r = 0.646$ ,  $F_{1,107} = 76.69$ ,  $P < 0.001$ ,  $\text{coh}_{\text{normal}} = 0.646 + \text{coh}_{\text{collapsed}} \times 0.954$ ). Accordingly, instead of 0.6, we used 1.2 as the coherence inclusion criterion for the linear-track sessions. For cells that had place fields during running in both directions on the track, the fields were analyzed separately. This is in accordance with the established directionality and independence of place fields in linear-track tasks.

**Cross-correlogram analysis.** Cell-pair cross-correlograms are histograms representing the probability that cell B will fire at time  $t$  relative to cell A in a 180-ms window. This window size is large enough to observe theta modulation of cells in the 7–8-Hz range that is typical of active exploration at 19–21 °C. Data from all cells for a given rat were combined and then the rat average was used for further analyses. The CCGP closest to zero was found after applying a cubic spline function to the raw data. The position of this peak represents the temporal offset of cell B relative to cell A (CCGP shift) in any given theta cycle. A negative shift indicates that cell B fires before A and a positive shift indicates the opposite.

**Heading prediction.** We used a method that is related to that used for position reconstruction (**Supplementary Methods**) to predict the rat's momentary heading. The first half of each recording session was used to build the model, which was then used to predict heading in the second half of the session. For each cell, we counted the number of spikes fired while the rat was moving at a particular angle relative to the cell's place-field peak (peak angle). This was repeated for spikes firing in 60°-wide theta bands centered at 0, 60, 120, 180, 240 and 300°. Spike counts were sorted into 36 peak-angle bins converted into firing probabilities, creating a separate peak-angle tuning curve for each theta-phase band. During reconstruction, the average position and heading of the rat was calculated in a 400-ms sliding window centered on the time of each position sample. Each action potential in the window contributed a peak-angle probability histogram that was appropriate to the cell and the firing-phase band. To convert angle probabilities from a place field-centered coordinate system to a camera-centered one, we shifted each histogram by the angle separating the rat's current location from the field peak. This is justified on the assumption that the rat carries an accurate representation of its current location and the geometric relationship between different locations in the environment in its hippocampus<sup>1,2,44</sup>. Once corrected, the histograms from each spike were multiplied together to derive a cumulative probability histogram, corrected by the amount of time the rat spent at each peak angle (**Supplementary Fig. 4**). The peak of this histogram was taken as the most likely heading of the rat in the window. Heading-prediction windows were only included in subsequent analyses if they contained spikes from at least two cells.

**Prediction errors.** The heading-prediction error was the absolute value of the angular difference between the predicted and actual (mean) heading in a given window. Position-reconstruction error was the Cartesian distance (cm) between the predicted and actual position of the rat, again averaged in each prediction window. The mean error for all windows containing spikes in a given phase band was calculated for each rat, and the rat averages in each phase band were used for repeated-measures statistical comparisons.

*Note: Supplementary information is available on the Nature Neuroscience website.*

## ACKNOWLEDGMENTS

Thanks to N. Campo-Urriza and L. Norman for technical assistance. We also thank J. Huck, T. Klausberger, P. Magill and O. Paulsen for providing helpful comments on the manuscript. This work was supported by the Medical Research Council (UK). The D.Phil. studentship of T.J.S. and K.A. are funded by the Wellcome Trust (UK).



## AUTHOR CONTRIBUTIONS

J.R.H., T.J.S. and K.A. conducted the experiments. J.R.H. carried out the data analyses. J.R.H. and J.C. wrote the manuscript. J.C. supervised the project.

Published online at <http://www.nature.com/natureneuroscience>

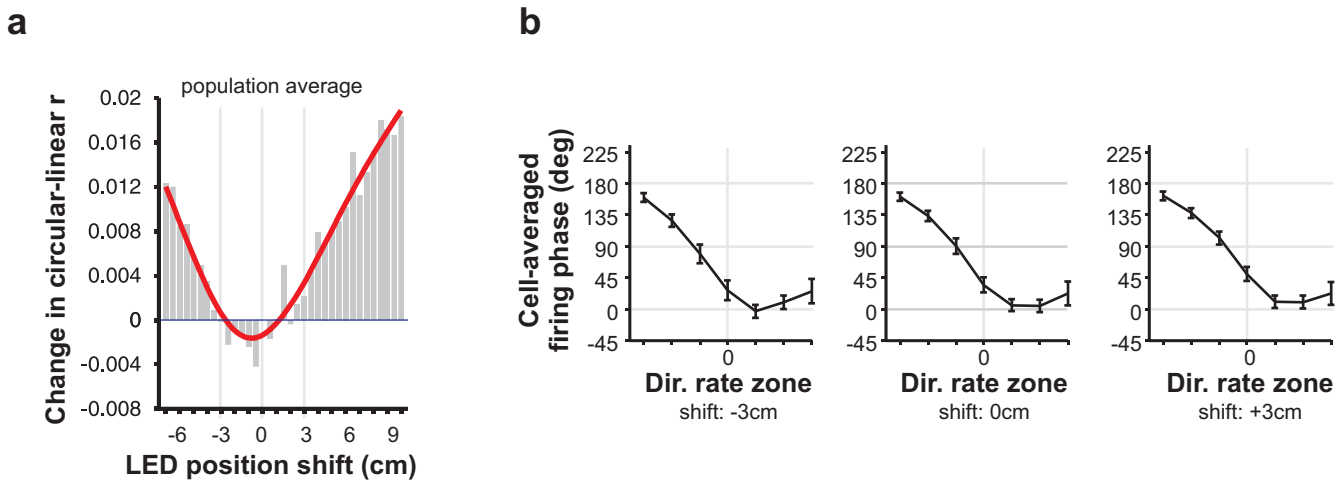
Reprints and permissions information is available online at <http://npg.nature.com/reprintsandpermissions>

1. O'Keefe, J. & Nadel, L. *The Hippocampus as a Cognitive Map* (Oxford University Press, Oxford, 1978).
2. Wilson, M.A. & McNaughton, B.L. Dynamics of the hippocampal ensemble code for space. *Science* **261**, 1055–1058 (1993).
3. Zhang, K., Ginzburg, I., McNaughton, B.L. & Sejnowski, T.J. Interpreting neuronal population activity by reconstruction: unified framework with application to hippocampal place cells. *J. Neurophysiol.* **79**, 1017–1044 (1998).
4. Whishaw, I.Q. & Vanderwolf, C.H. Hippocampal EEG and behavior: effects of variation in body temperature and relation of EEG to vibrissae movement, swimming and shivering. *Physiol. Behav.* **6**, 391–397 (1971).
5. O'Keefe, J. & Recce, M.L. Phase relationship between hippocampal place units and the EEG theta rhythm. *Hippocampus* **3**, 317–330 (1993).
6. Skaggs, W.E., McNaughton, B.L., Wilson, M.A. & Barnes, C.A. Theta phase precession in hippocampal neuronal populations and the compression of temporal sequences. *Hippocampus* **6**, 149–172 (1996).
7. Huxter, J., Burgess, N. & O'Keefe, J. Independent rate and temporal coding in hippocampal pyramidal cells. *Nature* **425**, 828–832 (2003).
8. Geisler, C., Robbe, D., Zugaro, M., Sirota, A. & Buzsáki, G. Hippocampal place cell assemblies are speed-controlled oscillators. *Proc. Natl. Acad. Sci. USA* **104**, 8149–8154 (2007).
9. Jensen, O. & Lisman, J.E. Position reconstruction from an ensemble of hippocampal place cells: contribution of theta phase coding. *J. Neurophysiol.* **83**, 2602–2609 (2000).
10. Foster, D.J. & Wilson, M.A. Hippocampal theta sequences. *Hippocampus* **17**, 1093–1099 (2007).
11. Dragoi, G. & Buzsáki, G. Temporal encoding of place sequences by hippocampal cell assemblies. *Neuron* **50**, 145–157 (2006).
12. O'Keefe, J. & Burgess, N. Dual phase and rate coding in hippocampal place cells: theoretical significance and relationship to entorhinal grid cells. *Hippocampus* **15**, 853–866 (2005).
13. Tsodyks, M.V., Skaggs, W.E., Sejnowski, T.J. & McNaughton, B.L. Population dynamics and theta rhythm phase precession of hippocampal place cell firing: a spiking neuron model. *Hippocampus* **6**, 271–280 (1996).
14. Lisman, J.E. Relating hippocampal circuitry to function: recall of memory sequences by reciprocal dentate-CA3 interactions. *Neuron* **22**, 233–242 (1999).
15. Hasselmo, M.E. What is the function of hippocampal theta rhythm? Linking behavioral data to phasic properties of field potential and unit recording data. *Hippocampus* **15**, 936–949 (2005).
16. Siapas, A.G., Lubenov, E.V. & Wilson, M.A. Prefrontal phase locking to hippocampal theta oscillations. *Neuron* **46**, 141–151 (2005).
17. Jones, M.W. & Wilson, M.A. Phase precession of medial prefrontal cortical activity relative to the hippocampal theta rhythm. *Hippocampus* **15**, 867–873 (2005).
18. Harris, K.D. *et al.* Spike train dynamics predicts theta-related phase precession in hippocampal pyramidal cells. *Nature* **417**, 738–741 (2002).
19. Jensen, O. & Lisman, J.E. Hippocampal CA3 region predicts memory sequences: accounting for the phase precession of place cells. *Learn Mem.* **3**, 279–287 (1996).
20. Wallenstein, G.V. & Hasselmo, M.E. GABAergic modulation of hippocampal population activity: sequence learning, place-field development and the phase-precession effect. *J. Neurophysiol.* **78**, 393–408 (1997).
21. Maurer, A.P., Cowen, S.L., Burke, S.N., Barnes, C.A. & McNaughton, B.L. Organization of hippocampal cell assemblies based on theta phase precession. *Hippocampus* **16**, 785–794 (2006).
22. Buzsáki, G. *Rhythms of the Brain* (Oxford University Press, Oxford, 2006).
23. Muller, R.U. & Kubie, J.L. The firing of hippocampal place cells predicts the future position of freely moving rats. *J. Neurosci.* **9**, 4101–4110 (1989).
24. Skaggs, W.E. & McNaughton, B.L. Replay of neuronal firing sequences in rat hippocampus during sleep following spatial experience. *Science* **271**, 1870–1873 (1996).
25. Burgess, N., Recce, M. & O'Keefe, J. A model of hippocampal function. *Neural Netw.* **7**, 1065–1081 (1994).
26. Harris, K.D., Csicsvari, J., Hirase, H., Dragoi, G. & Buzsáki, G. Organization of cell assemblies in the hippocampus. *Nature* **424**, 552–556 (2003).
27. Mehta, M.R., Lee, A.K. & Wilson, M.A. Role of experience and oscillations in transforming a rate code into a temporal code. *Nature* **417**, 741–746 (2002).
28. Yamaguchi, Y., Aota, Y., McNaughton, B.L. & Lipa, P. Bimodality of theta phase precession in hippocampal place cells in freely running rats. *J. Neurophysiol.* **87**, 2629–2642 (2002).
29. Diba, K. & Buzsáki, G. Forward and reverse hippocampal place-cell sequences during ripples. *Nat. Neurosci.* **10**, 1241–1242 (2007).
30. Greenstein, Y.J., Pavlides, C. & Winson, J. Long-term potentiation in the dentate gyrus is preferentially induced at theta rhythm periodicity. *Brain Res.* **438**, 331–334 (1988).
31. Debanne, D., Gähwiler, B.H. & Thompson, S.M. Long-term synaptic plasticity between pairs of individual CA3 pyramidal cells in rat hippocampal slice cultures. *J. Physiol. (Lond.)* **507**, 237–247 (1998).
32. Debanne, D., Guerineau, N.C., Gähwiler, B.H. & Thompson, S.M. Physiology and pharmacology of unitary synaptic connections between pairs of cells in areas CA3 and CA1 of rat hippocampal slice cultures. *J. Neurophysiol.* **73**, 1282–1294 (1995).
33. Bi, G.Q. & Poo, M.M. Synaptic modifications in cultured hippocampal neurons: dependence on spike timing, synaptic strength and postsynaptic cell type. *J. Neurosci.* **18**, 10464–10472 (1998).
34. Lisman, J.E., Talamini, L.M. & Raffone, A. Recall of memory sequences by interaction of the dentate and CA3: a revised model of the phase precession. *Neural Netw.* **18**, 1191–1201 (2005).
35. McNaughton, B.L. *et al.* Deciphering the hippocampal polyglot: the hippocampus as a path integration system. *J. Exp. Biol.* **199**, 173–185 (1996).
36. Samsonovich, A. & McNaughton, B.L. Path integration and cognitive mapping in a continuous attractor neural network model. *J. Neurosci.* **17**, 5900–5920 (1997).
37. Taube, J.S., Muller, R.U. & Ranck, J.B. Jr. Head-direction cells recorded from the postsubiculum in freely moving rats. I. Description and quantitative analysis. *J. Neurosci.* **10**, 420–435 (1990).
38. Sargolini, F. *et al.* Conjunctive representation of position, direction, and velocity in entorhinal cortex. *Science* **312**, 758–762 (2006).
39. Golob, E.J. & Taube, J.S. Head direction cells in rats with hippocampal or overlying neocortical lesions: evidence for impaired angular path integration. *J. Neurosci.* **19**, 7198–7211 (1999).
40. Maaswinkel, H., Jarrard, L.E. & Whishaw, I.Q. Hippocampectomized rats are impaired in homing by path integration. *Hippocampus* **9**, 553–561 (1999).
41. Sharp, P.E. & Green, C. Spatial correlates of firing patterns of single cells in the subiculum of the freely moving rat. *J. Neurosci.* **14**, 2339–2356 (1994).
42. Huerta, P.T. & Lisman, J.E. Bidirectional synaptic plasticity induced by a single burst during cholinergic theta oscillation in CA1 *in vitro*. *Neuron* **15**, 1053–1063 (1995).
43. Ang, C.W., Carlson, G.C. & Coulter, D.A. Hippocampal CA1 circuitry dynamically gates direct cortical inputs preferentially at theta frequencies. *J. Neurosci.* **25**, 9567–9580 (2005).
44. Muller, R.U., Kubie, J.L. & Sayppoff, R. The hippocampus as a cognitive graph (abridged version). *Hippocampus* **1**, 243–246 (1991).
45. Maurer, A.P. & McNaughton, B.L. Network and intrinsic cellular mechanisms underlying theta phase precession of hippocampal neurons. *Trends Neurosci.* **30**, 325–333 (2007).
46. Lengyel, M., Szatmari, Z. & Erdi, P. Dynamically detuned oscillations account for the coupled rate and temporal code of place cell firing. *Hippocampus* **13**, 700–714 (2003).
47. Giocomo, L.M., Zilli, E.A., Fransen, E. & Hasselmo, M.E. Temporal frequency of subthreshold oscillations scales with entorhinal grid cell field spacing. *Science* **315**, 1719–1722 (2007).
48. Buzsáki, G. Theta oscillations in the hippocampus. *Neuron* **33**, 325–340 (2002).
49. Magee, J.C. Dendritic mechanisms of phase precession in hippocampal CA1 pyramidal neurons. *J. Neurophysiol.* **86**, 528–532 (2001).
50. Fisher, N.I. *Statistical Analysis of Circular Data* (Cambridge University Press, Cambridge, 1993).

## Supplementary Figures

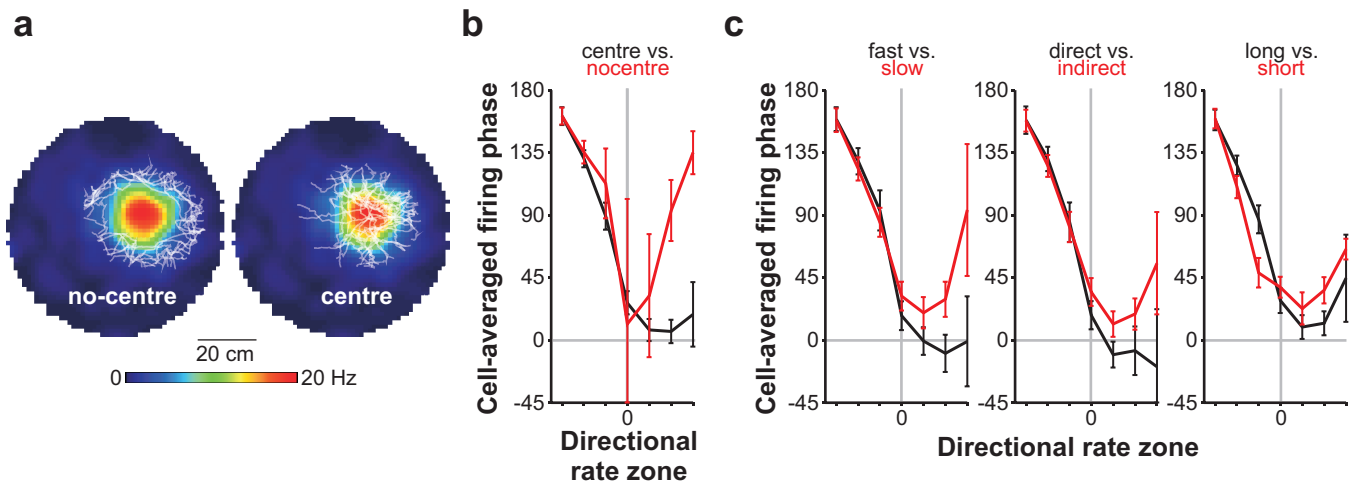
**Manuscript title:** Theta phase-specific codes for two-dimensional position, trajectory and heading in the hippocampus

**Authors:** John R. Huxter, Timothy J. Senior, Kevin Allen, and Jozsef Csicsvari

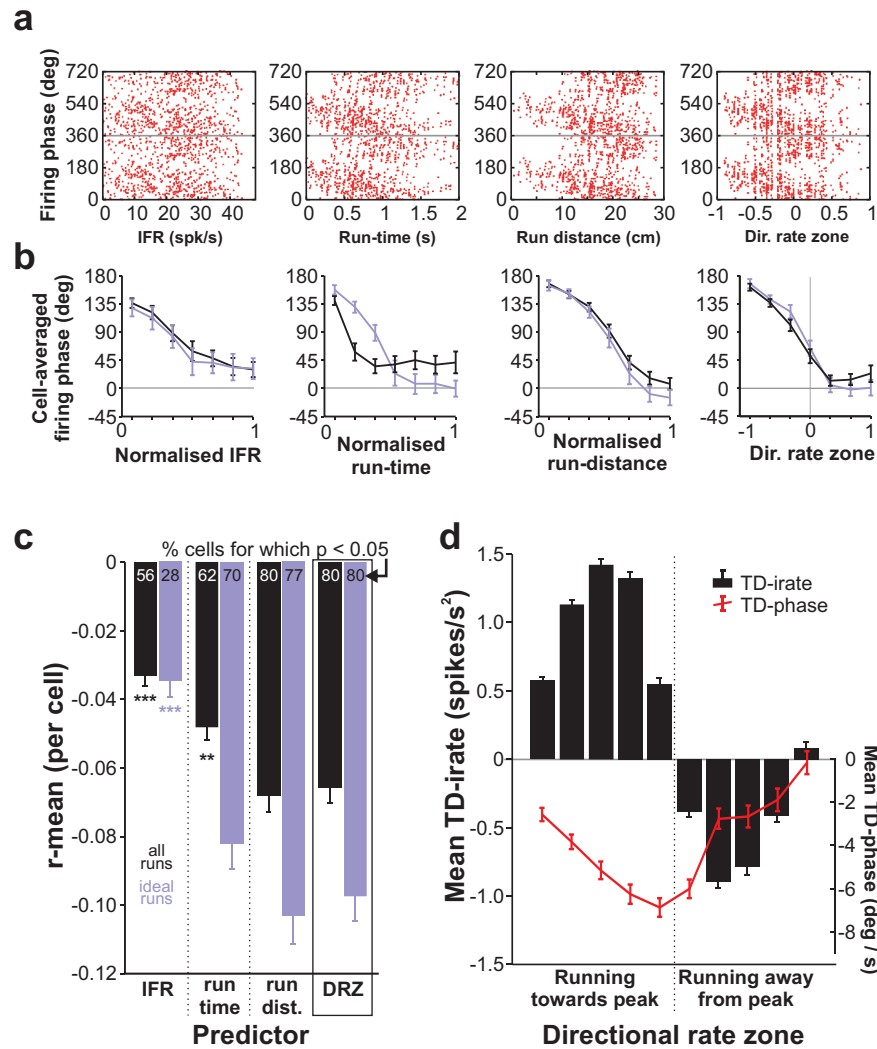


### Supplementary Figure S1 | Small LED position corrections have little effect on phase precession.

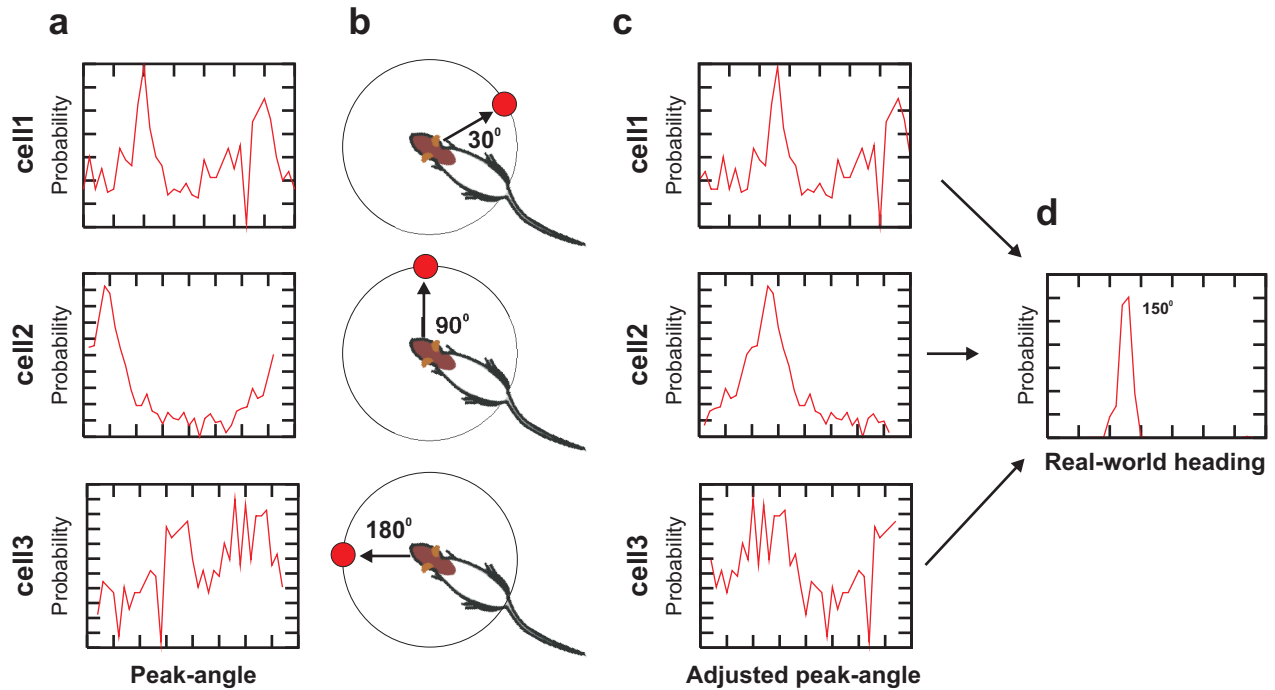
Similar to the analysis of place field size in Figure 1, we looked at the effect that correcting potential misplacement of the LED had on the linear-circular correlation between directional rate zone (DRZ) and theta firing phase. **a**, The effect of shifting the LED position forward or backwards along the axis of the rat's head in 0.5 cm increments. Negative changes in the linear-circular correlation indicate improved phase precession. In contrast to place field size, the best reduction coincides with a 0.5 cm backwards correction, as indicated by the minimum in the spline-fit of the data (red line). **b**, The effect of shifting LED position forwards or backwards 3 cm on the population phase precession profile. The 3 cm shift was the one applied to all other data in the current experiment, as it minimises place field size. Note however that the phase precession profiles are virtually identical. This suggests that our phase precession results are essentially insensitive to such small changes in apparent LED position, and that the 0.005 improvement in the linear-circular regression coefficient which would have been achieved by shifting positions backwards instead of forwards is of little consequence. Note however that had our actual LED placement been different (say, even further posterior on the rat's head) the correction might well have been relevant.



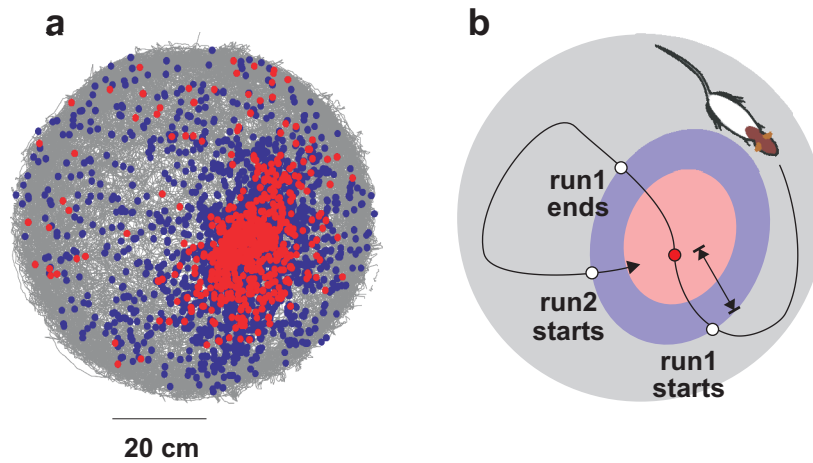
**Supplementary Figure S2 | Effects of behaviour on phase precession.** We asked whether behavioural aspects of runs through the place field affected phase precession based on directional rate zone (DRZ). **a**, An example of runs through a place field which include (left) or omit (right) the place field centre. **b**, A comparison of runs which include/omit the field centre. Clearly, if the rat skirts the edge of the place field, firing phase fails to shift to the earliest parts of the theta cycle as the rat exits. This helps in part to explain the increased variance in firing phase as the rat exits the field - the combined data in Figures 1g and 3a includes many runs when the rat does not pass through the place field centre. Error bars are 95% C.I. **c**, Comparison of DRZ phase precession for fast/slow, direct/indirect, and long/short runs through place fields. Criteria were based on the upper and lower 25th percentile of the range of each predictor, and only runs through the field centre used. Indirect runs are the most meandering ones (see Supplementary Methods for details). Error bars are 95% circular C.I. As with peripheral runs but to a lesser extent, very slow or meandering runs produce a truncated precession. Both very long (presumably meandering) and very short (almost missing the field centre) runs produce truncated precession. Together the results suggest that while phase precession does not require stereotyped movement through the place field, it suffers when the rat takes extremely complicated trajectories or slows/stops in the place field.



**Supplementary Figure S3 | Comparison of different firing phase predictors.** We compared the quality of spatial and non-spatial predictors of the theta firing phase of place cells. **a**, For one place cell, plots of firing phase versus each of instantaneous firing rate (IFR), run-time, run-distance, and directional rate zone (DRZ). Except for DRZ, predictor values above the 95th percentile are treated as outliers and excluded. Data were only taken from “ideal” runs through the field centre which are faster and follow less tortuous paths than most (cutoff = median values). Note that this is more inclusive than the “restricted-run” criterion used in Figure 3, where the upper and lower 25th percentiles were used as the velocity and tortuosity cutoffs, respectively. **b**, In order to calculate the population averages for the same measures, data was normalised to the minimum and maximum predictor values occurring within the place field and sorted into seven bins. Here phase precession based on all (black) or only ideal (purple) runs through the field is shown. The greatest sensitivity to inclusion of “non-ideal” runs is found with the run-time phase precession. Error bars are 95% CI. **c**, A comparison of the mean linear-circular r-values for firing phase as a function of each predictor. Results are based only on cells contributing at least 100 spikes to the correlation. The correlation between IFR and firing phase was significant for only 75/133 cells, making it the weakest of the predictors tested. Error bars are SEM.  $**p < 0.01$ ,  $***p < 0.001$ , Tukey’s HSD, comparisons are with DRZ scores. **d**, Across DRZs, the temporal derivative of IFR and phase tend to dissociate. Changes in phase (red) are consistently negative in all rate zones, while firing rate (black) changes are positive as the rat approaches the field centre (negative DRZ) and negative as the rat runs away (positive DRZ). That is, while spike trains shift from accelerating to decelerating mode, phase precession continues even as the rat exits the field. Temporal derivatives were calculated using a sliding window spanning 3-theta-cycles. Error bars are SEM.



**Supplementary Figure S4 | Combining tuning curves for heading prediction.** **a**, The peak-angle tuning curves appropriate to the firing phase band of three cells which were active in a given 400 ms prediction window. That is, given that the cell fired at theta phase  $p$ , what is the probability that the rat is heading at a given angle, relative to the peak of the field? **b**, The histograms are adjusted by the angle separating the rat's current location from the position of the cell's place field centre (red circle). This converts the peak-angle histogram to a real-world direction histogram. **c**, The adjusted histograms for the three cells. **d**, The product of the three probability histograms yields single sharply-peaked histogram representing the most likely heading of the rat. In this simulation, the rat is actually heading at  $150^\circ$ , so the prediction is perfectly accurate.



**Supplementary Figure S5 | Broad spatial distribution of firing phases, and run-definition. a,** The distribution of spikes from a representative place cell. Spikes firing on the trough (red) and ascending-slope (blue) of theta cycles broadly fire in the centre and perimeter of the place field, respectively. Hence trough-firing cells show greater spatial selectivity. Spikes are superimposed on the path of the rat. **b,** Definition of “runs” for the purpose of analyzing phase precession in 2D. The coloured zone represents the place field of the cell in **a**, with runs beginning upon entry to the field and ending upon exit. For a given action potential (red circle) run-distance ( ) is the cumulative distance connecting position samples between the start of the run and the time of the spike.

## Supplementary Methods

**Manuscript title:** Theta phase-specific codes for two-dimensional position, trajectory and heading in the hippocampus

**Authors:** John R. Huxter, Timothy J. Senior, Kevin Allen, and Jozsef Csicsvari

### *Unit isolation and selection*

Unit isolation and clustering procedures have been described before<sup>1</sup>. For further analysis, we used only units with clear refractory periods in their autocorrelation and well defined cluster boundaries. In addition, we calculated cluster isolation distances (based on Mahabalanis distance) to ensure that the selected spike-clusters did not overlap during the course of the recordings<sup>2</sup>. Pyramidal cells and interneurons were discriminated by their autocorrelations, firing rate and wave forms, as previously described<sup>3</sup>. Only pyramidal cells with mean firing rates < 10 spikes/s were considered for this study. In order to exclude cell firing during sharp wave/ripple oscillations associated with immobility, data were only used from periods when the rat was moving at >5 cm/s.

### *Spatial firing rate maps*

We divided the camera view into a 2-dimensional array of bins, each representing a 2.5 X 2.5 cm area of the floor. Firing rates in each bin were taken as the number of spikes fired in the bin divided by the total time spent there. *Coherence* reflects the similarity of the firing rate in adjacent bins, and is the z-transform of the correlation between the rate in a bin and the average rate of its eight nearest neighbours<sup>4</sup>. *Sparsity* corresponds with the proportion of the environment in which a cell fires, corrected for dwell time<sup>5</sup>, and is defined as  $(\sum P_i R_i)^2 / \sum P_i R_i^2$ , where  $P_i$  is the probability of the rat occupying bin  $i$ ,  $R_i$  is the firing rate in bin  $i$ . We only included cells for analysis if they had a mean firing rate (total spikes / session duration) of less than 10 spikes/s and if their unsmoothed firing rate maps had a coherence of at least 0.6 and sparsity of no more than 0.3. The rate map was then smoothed using a 9 X 9 bin Gaussian kernel, which compensated for limits on recording time while preserving the overall size and shape of the region where the cell tended to fire. The map bin with the highest firing rate defined the peak firing rate for the cell. The place field for each cell was the set of contiguous bins with rates >10% of the peak bin rate. The peak-zone was defined as the upper 80<sup>th</sup> rate-percentile of in-field bins. Note that the peak-zone therefore represents 20% of the place field, and so can include bins in which firing rate is less than 80% of the peak firing rate.

### *Position correction*

The point we take as an indication of the rat's position is somewhat arbitrary and may not reflect the "true" position from the rat's perspective<sup>4,5</sup>. This is evident when place fields are plotted from data collected during different movement directions, where it can be seen that the fields shift depending on the direction of motion, and usually in the opposite direction (**Fig. 1**). Consequently, we corrected the rat's position along the anterior-posterior axis of its head, as defined by the orientation of the LED array. First we applied a series of forward and backward shifts to the position record, ranging from -7 to 10 cm, in 0.5 cm steps. The optimal correction was chosen based on the assumption that the "correct" positioning of the LED array would lead to the most compact place fields<sup>5</sup>. For

each rat, a cubic spline function was fit to the plot of mean field size versus position shift, and the minimum of the function was taken as the optimal correction. The optimal shifts ranged from 2.5 to 3.5 cm, except for one animal where the minimum was 1cm. In this case the plot was sparse due to the small number of cells recorded, but the LED array (and its position on the head) was the same for this rat as the others. A plot which averaged the field size change for all cells from all animals yielded a minimum for 3 cm shifts, so this correction was applied to all rats. This placed the corrected LED location approximately above the rat's nose. The corrected data was used for all subsequent analyses.

### *Theta detection and firing phase*

For each rat, we used one of the tetrodes in the CA1 pyramidal cell layer to detect theta EEG oscillations. Off-line, we passed the EEG signal through a bidirectional digital Butterworth filter (2 Hz high-pass) and averaged with a 21ms sliding window to remove high-frequency components. A sine wave was fitted to the interval between pairs of positive-to-negative zero crossings in the filtered EEG signal, provided the interval fell within the theta frequency range (5–12 Hz). Phase “zero” was defined as the first zero-crossing. The goodness-of-fit (mean square error <0.6) was used to detect the presence of a theta cycle. The firing phase of a spike in degrees is the elapsed fraction of the current cycle at the time of the spike, scaled to a 0–360 range<sup>6</sup>.

### *Behavioural effects on phase precession*

In addition to running slowly or quickly through the place field, during 2D exploration the rat is also free to make passes through the place field which exclude the field centre, take complicated trajectories, and which may vary in length. We compared phase precession under each predictor for all runs as compared with “ideal” runs through the field (**Fig. 3**). Ideal runs are those for which the rat crosses the field peak-zone, running speed is above the median for runs through that field, and the circular standard deviation<sup>7</sup> of the rat's heading is below the median. In other words, ideal runs are fairly fast, fairly straight, and include the middle of the place field.

For each cell we also compared DRZ phase precession on runs which included or excluded the place field peak-zone, and runs which were in the upper versus the lower 25<sup>th</sup> percentile on measures of a) speed during the run and b) the standard deviation of heading during the run. We calculated the circular mean<sup>7</sup> firing phase of the cell in each DRZ under each condition. Data for all cells were combined, omitting cases where the mean was based on < 20 runs or the variance was too high for the mean phase to be meaningful.

### *Position reconstruction*

The smoothed place cell firing rate maps from the first half of each recording session were used to calculate the probability of each cell firing in a given bin representing a 2.5 X 2.5 cm region of the environment. For the second half of each session we used a 400 ms sliding prediction window and a Bayesian maximum likelihood method<sup>8,9</sup> to reconstruct positions, based on the following formula:

$$P(\mathbf{x}|\mathbf{n}) = C(\boldsymbol{\tau}, \mathbf{n})P(\mathbf{x}) \left( \prod f_i(\mathbf{x})^{n_i} \right) \exp(-\boldsymbol{\tau} \sum f_i(\mathbf{x}))$$

... where  $P(\mathbf{x}|\mathbf{n})$  is the probability of the rat occupying bin  $\mathbf{x}$  given the cell activity in the window. The peak in this distribution is taken as the predicted position.  $P(\mathbf{x})$  is the mean

probability of the rat occupying position  $\mathbf{x}$ .  $f_i(\mathbf{x})$  is the probability of the cell  $i$  firing in map bin  $\mathbf{x}$ , which equates with the average firing rate of the cell in that bin.  $n_i$  is the number of spikes from cell  $i$  in the sliding window, and  $\tau$  is the size of the sliding window.  $C(\tau, \mathbf{n})$  is a normalization factor calculated so that the sum of the probabilities for each bin = 1. No attempt was made to prevent “jumpy” reconstruction or to smooth the reconstructed position values.

## References

1. Csicsvari, J., Hirase, H., Czurko, A. & Buzsaki, G. Reliability and state dependence of pyramidal cell-interneuron synapses in the hippocampus: an ensemble approach in the behaving rat. *Neuron* **21**, 179-189 (1998).
2. Harris, K.D., Hirase, H., Leinekugel, X., Henze, D.A. & Buzsaki, G. Temporal interaction between single spikes and complex spike bursts in hippocampal pyramidal cells. *Neuron* **32**, 141-149 (2001).
3. Csicsvari, J., Hirase, H., Czurko, A., Mamiya, A. & Buzsaki, G. Oscillatory coupling of hippocampal pyramidal cells and interneurons in the behaving Rat. *J Neurosci* **19**, 274-287 (1999).
4. Muller, R.U. & Kubie, J.L. The firing of hippocampal place cells predicts the future position of freely moving rats. *J Neurosci* **9**, 4101-4110 (1989).
5. Skaggs, W.E., McNaughton, B.L., Wilson, M.A. & Barnes, C.A. Theta phase precession in hippocampal neuronal populations and the compression of temporal sequences. *Hippocampus* **6**, 149-172 (1996).
6. Huxter, J., Burgess, N. & O'Keefe, J. Independent rate and temporal coding in hippocampal pyramidal cells. *Nature* **425**, 828-832 (2003).
7. Fisher, N.I. *Statistical Analysis of Circular Data* (Cambridge University Press, Cambridge, 1993).
8. Jensen, O. & Lisman, J.E. Position reconstruction from an ensemble of hippocampal place cells: contribution of theta phase coding. *Journal of neurophysiology* **83**, 2602-2609 (2000).
9. Zhang, K., Ginzburg, I., McNaughton, B.L. & Sejnowski, T.J. Interpreting neuronal population activity by reconstruction: unified framework with application to hippocampal place cells. *Journal of neurophysiology* **79**, 1017-1044 (1998).